Functional genomic analysis unravels a metabolic-inflammatory interplay in adrenoleukodystrophy

Agatha Schlüter[1,2], Lluís Espinosa[3], Stéphane Fourcade[1,2], Jorge Galino[1,2], Eva López[1,2], Ekaterina Ilieva[1,2], Laia Morató[1,2], Muriel Asheuer[4], Ted Cook[5], Alistair McLaren[5], Juliet Reid[5], Fiona Kelly[5], Stewart Bates[5], Patrick Aubourg[4], Elena Galea[6,7] and Aurora Pujol[1,2,7,*]

[1]Neurometabolic Diseases Laboratory and Institut de Neuropatologia de Bellvitge (IDIBELL), L'Hospitalet de Llobregat, 08908 Barcelona, Spain, [2]Centro de Investigación en Red sobre Enfermedades Raras (CIBERER), Spain, [3]Institut Municipal d'Investigacions Mèdiques-Hospital del Mar, 08003 Barcelona, Spain, [4]INSERM, U745 and University René Descartes Paris 5, Hôpital Saint-Vincent de Paul, Paris, France, [5]GSK Medicines Research Centre, Stevenage, Hertfordshire SG1 2NY, UK, [6]Institut de Neurociències, Universitat Autònoma de Barcelona, 08193 Barcelona, Spain, and [7]Institució Catalana de Recerca i Estudis Avançats (ICREA), Barcelona, Spain

X-linked adrenoleukodystrophy (X-ALD) is an inherited disorder characterized by axonopathy and demyelination in the central nervous system and adrenal insufficiency. Main X-ALD phenotypes are: (i) an adult adrenomyeloneuropathy (AMN) with axonopathy in spinal cords, (ii) cerebral AMN with brain demyelination (cAMN) and (iii) a childhood variant, cALD, characterized by severe cerebral demyelination. Loss of function of the ABCD1 peroxisomal fatty acid transporter and subsequent accumulation of very-long-chain fatty acids (VLCFAs) are the common culprits to all forms of X-ALD, an aberrant microglial activation accounts for the cerebral forms, whereas inflammation allegedly plays no role in AMN. How VLCFA accumulation leads to neurodegeneration and what factors account for the dissimilar clinical outcomes and prognosis of X-ALD variants remain elusive. To gain insights into these questions, we undertook a transcriptomic approach followed by a functional-enrichment analysis in spinal cords of the animal model of AMN, the _Abcd1_$^-$ null mice, and in normal-appearing white matter of cAMN and cALD patients. We report that the mouse model shares with cAMN and cALD a common signature comprising dysregulation of oxidative phosphorylation, adipocytokine and insulin signaling pathways, and protein synthesis. Functional validation by quantitative polymerase chain reaction, western blots and assays in spinal cord organotypic cultures confirmed the interplay of these pathways through IkB kinase, being VLCFA in excess a causal, upstream trigger promoting the altered signature. We conclude that X-ALD is, in all its variants, a metabolic/inflammatory syndrome, which may offer new targets in X-ALD therapeutics.

INTRODUCTION

X-linked adrenoleukodystrophy (X-ALD: McKusick no. 300100) is a neurometabolic genetic disorder characterized by progressive demyelination within the central nervous system (CNS), axonopathy in spinal cords and adrenal insufficiency. It is the most common monogenic leukodystrophy and peroxisomal disorder with a minimum incidence of 1 in 17 000

males. The disease is caused by mutations in the ABCD1 (ALD) gene (Xq28) encoding for the peroxisomal ABC transporter (1,2), which functions as a transporter of very-long-chain fatty acids (VLCFAs) or VLCFA−CoA esters into the peroxisome for degradation by β-oxidation (3).

Three major disease variants have been described: a late-onset form affecting adults and called adrenomyeloneuropathy (AMN) as it presents peripheral neuropathy and distal

*To whom correspondence should be addressed at: Neurometabolic Diseases Laboratory, IDIBELL, Hospital Duran i Reynals 3ª planta, Gran Via 199, 08908 L'Hospitalet de Llobregat, Barcelona, Spain. Tel: +34 932607343; Fax: +34 932607414; Email: apujol@idibell.cat

axonopathy in spinal cord with secondary demyelination—but no brain demyelination—with spastic paraparesis as major symptoms, and two ultimately lethal forms, with cerebral demyelination and neuroinflammation, an adult form called cAMN, and an acute, childhood cerebral form called cALD. Interestingly, all clinical phenotypes can occur within the same family, that is, there is no phenotype–genotype correlation (4). All X-ALD patients indeed accumulate saturated VLCFAs and to a lesser extent, monounsaturated VCLFAs in plasma and tissues, most notably in the brain and adrenal cortex (5). VLCFAs are incorporated in complex lipids in cell membranes and are thought to destabilize and break myelin sheaths by occupying the lateral chains of proteolipid proteins, gangliosides and phospholipids (5). Although disease severity correlates with increased VLCFA contents in white matter (6), it remains elusive how the excess of VLCFAs causes the adrenal and spinal cord pathologies, while acting or not as a trigger of central demyelination. Thus, additional pathogenic factors critically shaping the clinical manifestation of X-ALD ought to exist. The identification of these factors is one of the outstanding questions in X-ALD and is essential to develop effective therapies.

Immunohistological analyses may provide clues as to missing links between fatty acid accumulation and pathology. Thus, a robust inflammatory response occurs in the brain white matter in cALD, whereas minimal or no inflammatory lesions have been reported in tissues from AMN patients (5). Moreover, a striking recovery has been recently described in cALD patients upon infusion of genetically corrected hematopoietic stem cells (7). This finding lends strong credence to the idea that microglia-driven inflammation causes cALD and prompts the question: how does the metabolic dysfunction lead to axonal damage and/or aberrant inflammation?

The mouse model of X-ALD is a classical knockout of the *Abcd1* gene, but it does not reproduce the phenotypic variability observed in X-ALD patients, because it only exhibits a late-onset neurodegenerative phenotype with axonopathy in spinal cords and peripheral nerves, resembling a mild AMN phenotype. The first immunohistochemical evidence of axonal degeneration and myelin pathology is detectable in the mouse spinal cord after 20 months of age, but not in the brain. This is concomitant to motor coordination impairment, disability and slowing of peripheral nerve conduction velocities (8,9). As observed in ALD patients, *Abcd1*-deficient mice accumulate VLCFAs in the brain and the spinal cord (10,11).

The *Abcd1⁻*-deficient mice thus provide a valuable model to establish the molecular profile of X-ALD at its earliest, presymptomatic stages, wherein pathogenic factors presumably build on. Likewise, we reason that tissues from non-affected brain areas of X-ALD patients are key to accessing causative events in disease pathogenesis. Thus, by using genome expression profiling and data mining of differentially expressed genes, we have identified dysregulated pathways in the spinal cord of *Abcd1⁻* mice and in non-affected white matter tissue of X-ALD patients. The analysis unravels a common metabolic abnormality signature both in the mouse model and human patients, characterized by mitochondrial dysregulation, insulin desensitization and an NF-κB-mediated proinflammatory response. A literature perusal points to the

IκB kinase (IKK) as a hub linking these pathways. Thus, IKK is activated by Toll-like receptors (TLRs) leading, on the one hand, to insulin desensitization and, on the other hand, to activation of NF-κB-dependent genes. Adipocytokines, in turn, are strong inhibitors of TLR signaling. By the combined use of quantitative polymerase chain reaction (q-PCR) and western blots, we did confirm in the mice the activation of the TLR-IKK-NF-κB axis and the reduction in insulin sensitization, concomitant to a decrease in the plasma contents of the adipocytokines leptin and adiponectin. These findings challenge the notion that inflammatory reactions only occur in severe forms of X-ALD and provide a basis to argue that a mostly benign inflammatory reaction initiated by VLCFAs may adopt an aggressive profile should a second hit appear (12). Overall, our transcriptomic analysis gives insights into the different molecular mechanisms operating in X-ALD phenotypes and provides clues as to mechanisms underlying the VLCFA-mediated inflammatory responses. This may help to develop therapeutic strategies to arrest the development of AMN into lethal forms.

RESULTS

We have analyzed: (i) spinal cords from *Abcd1⁻* mice at 3.5, 12 and 22 months of age to assess disease progression, (ii) non-affected white matter from children with cALD and (iii) non-affected white matter from adults with cAMN. In all cases, samples from age-matched healthy individuals were used as controls. First, mouse RNA probes were hybridized to an array that consisted of 20 736 mouse cDNA clones representing ∼15 000 Unigene clusters, whereas human material was hybridized to an Affymetrix Human Genome U133A Array including 22 283 probe sets comprising 14 500 expressed sequence tags from human genes. We found differential gene expression between X-ALD samples and controls upon using statistical linear models (see Materials and Methods) to compare transcriptomic profiles of each genotype and age. Next, we analyzed the functional enrichment of gene ontology (GO) terms (http://www.geneontology.org) (13), and the metabolic and cell signaling pathways extracted from the Kyoto Encyclopedia of Genes and Genomes (KEGG) (http ://www.genome.jp/kegg/) (14). Finally, we identified the X-ALD disease progression and signature common to mice and patients based on the enrichment in biological functions extracted from the previous analysis (Figure 1).

Definition of ALD *disease progression* and *signature* in mice by GO and KEGG enrichment analyses

As shown in Supplementary Material, Figure S1, GO terms significantly enriched in *Abcd1⁻* mice at all ages were: (i) metabolism with a prevalence of carbohydrate (tricarboxylic acid cycle: GO:0006099; malate: GO:0006108, GO:0016615; pyruvate metabolism: GO:0004743) and lipid metabolism (fatty-acid synthase: GO:0004312; acyl-ACP thioesterase: GO:0010281; lipid phosphatase activities: GO:0042577); (ii) mitochondrial function with a focus on the respiratory chain: GO:0006120, GO:0008121, GO:0008137, GO:0051539, GO:0005743, GO:0005739, GO:0005746; and (iii)
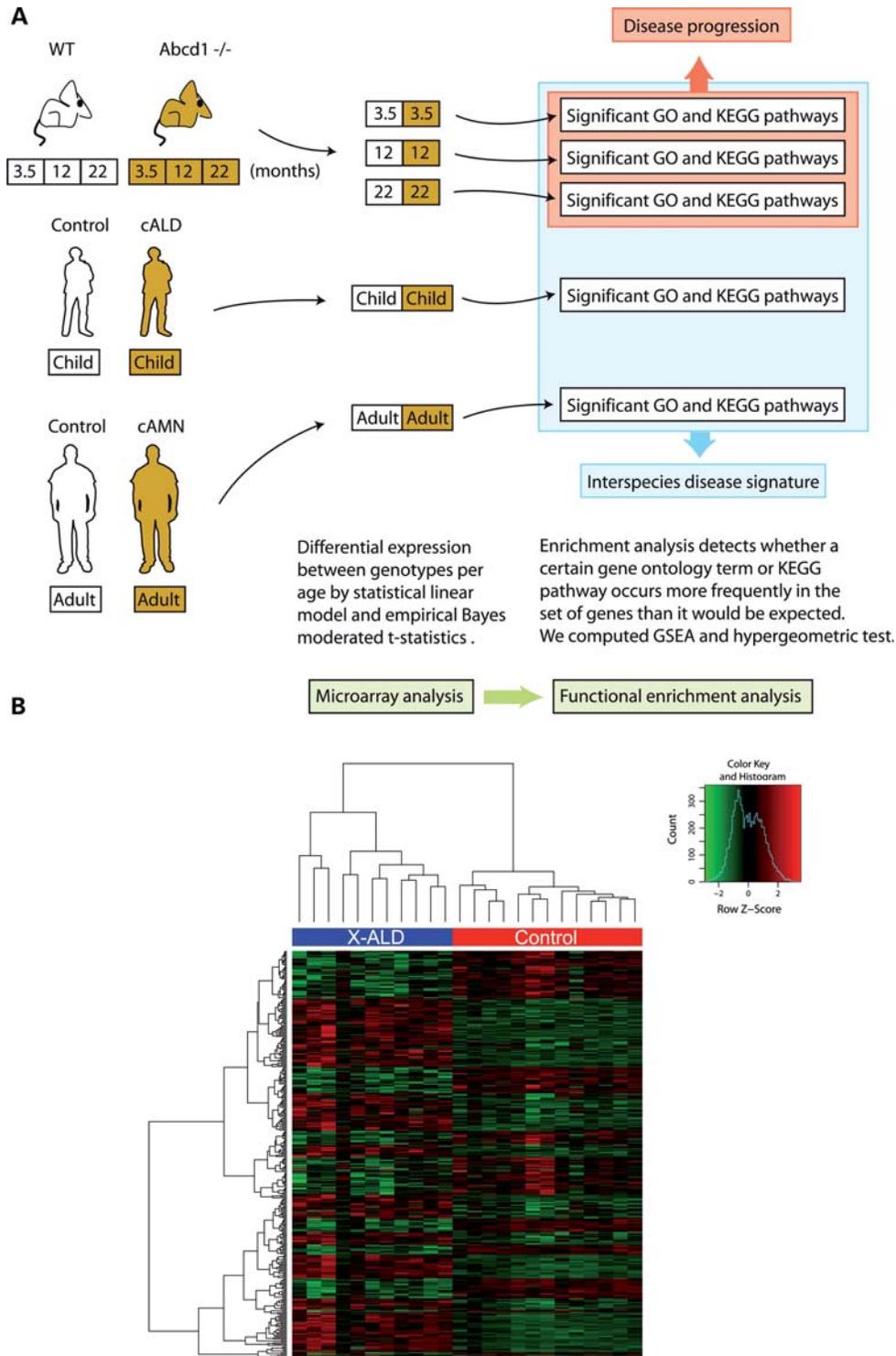
Figure 1. (**A**) A procedural diagram that indicates the pipeline followed to obtain the disease signature and progression in X-ALD mice and patients. (**B**) A hierarchical clustering heat-map of the expression intensities of the significantly regulated transcripts (on the *Y*-axis) versus the X-ALD patients and controls arrays (on the *X*-axis). Interestingly, we observed a clear separation between X-ALD patients and controls suggesting that hX-ALD pathology is concomitant to an alteration of transcriptional profiles.

transcriptional regulation involving ribosome: GO:0042254, GO:0003735, GO:0005840, GO:0015935, GO:0005843; translational elongation: GO:0006414, GO:0003746, GO:0005853 and ribonucleoprotein complex: GO:0030529.

As shown in Supplementary Material, Figure S2, we obtained the KEGG metabolic (S2A) or signaling (S2B) pathway enrichment in ALD mice at the three ages, by using either gene set enrichment analysis (GSEA) or

hypergeometric distribution function statistical analyses. A most remarkable finding is that many pathways were changed at 3.5 months, more than 1 year prior to the first neuropathological signs. Most of the pathways changed their expression over time following an up-down pattern whereby there was upregulated expression at 3.5 months of age, perhaps as a result of a compensatory mechanism that cannot be sustained for a long time, with the subsequent down-regulation at 12 months. Examples are: oxidative phosphorylation (OXPHOS system), 00190; glycolysis, 00010; citrate cycle (TCA cycle), 00020; proteasome, 03050; and ribosome, 03010 pathways. Regarding late-disease events, at 22 months, we found: (i) inflammatory response related to TGFβ: 04350 and T-cell receptor: 04660 signaling pathways activation, (ii) activation of the mammalian target of rapamycin complex-1 (mTORC1): 04150 and (iii) activated autophagic response: 04140, presumably as a result of an increase in cell debris removal associated with tissue damage. Supplementary Material, Figure S3 shows complete gene expression of selected pathways with up-down profiles.

We define the X-ALD *signature* as the metabolic (S2A) or signaling (S2B) pathways dysregulated at all ages under study. Dysregulated metabolic pathways include: (i) carbohydrate metabolism impairment with particular dysregulation of butanoate metabolism: 00650, TCA cycle: 00020, and glyoxylate and dicarboxylate metabolism: 00630; (ii) lipid metabolism impairment with fatty acid metabolism: 00071, glycerophospholipid metabolism: 00564 and sphingolipid metabolism: 00600 affected; (iii) amino acid metabolism dysregulation with valine, leucine and isoleucine degradation: 00280; (iv) glycan metabolism with glycan structures degradation: 01032 and focused on *N*-glycan degradation: 00511; and (v) unbalanced energy expenditure with altered OXPHOS: 00190 system.

Regarding the signaling pathways, the signature is characterized by the dysregulation of adipocytokine: 04920, insulin: 04910, mitogen-activated protein kinase: 04010 and the TLR: 4620 signaling pathways. Other dysregulated pathways are involved in protein and transcript processing such as aminoacyl-tRNA biosynthesis: 00970, proteasome: 03050, protein export: 03060 and ribosome: 03010.

Definition of ALD *signature* in human samples

We set out to investigate transcriptome changes in brain white matter that was disease-free by histopathological inspection with Luxol fast blue (LFB) staining to detect normal-looking areas as described (6,15). Evaluation of KEGG significant pathways in the differentially expressed transcriptome from child and adult X-ALD patients revealed the following dysregulated pathways (S4): (i) unbalanced energy expenditure with OXPHOS: 00190, insulin: 04910 and adipocytokine: 04920 pathways altered; (ii) cell communication impairment with focal adhesion: 04510 and adherens junction: 04520 dysregulation; (iii) common dysregulated pathways involved in protein and transcript processing such as aminoacyl-tRNA biosynthesis: 00970 and ribosome: 03010; (iv) protein degradation by ubiquitin-mediated proteolysis: 04120; (v) immune system response with complement and coagulation cascades pathway: 04610 and antigen processing and presentation pathway: 04612 activation; and (vi) induction of the
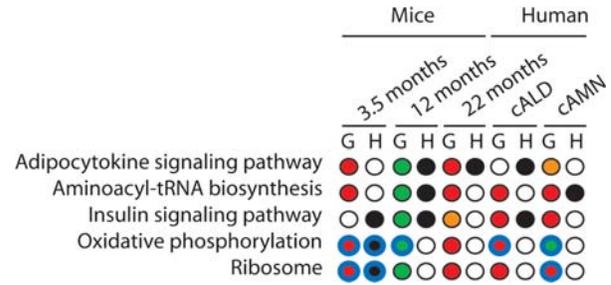

Figure 2. Common dysregulated pathways in spinal cords of ALD mice at 3.5, 12 and 22 months, and cerebral white matter of child and adult ALD patients. Significant KEGG pathways were identified by using the statistics gene set enrichment analysis (GSEA) (*G*) and hypergeometric distribution function (*H*). Only the pathways statistically significant in at least two tests are represented. Black spots represent dysregulated pathway when probability value *P* is <0.05 according to the *H*-test, which detects changes but does not inform about their up or down direction. Red and green spots represent up- and down-regulated pathway expression based on the *G*-test when probability value of *P* is <0.05, orange spots means dysregulated pathway based on the *G*-test with a probability value of <0.05, in case the gene set does not have a clear tendency to be up- or downregulated. Blue circle means significant pathway with a probability value of *P* < 0.0001.

antioxidant response with affected expression of the glutathione (GSH) metabolism pathway: 00480. The following pathways were thus dysregulated in both *Abcd1⁻* mouse and human X-ALD: (i) adipocytokine signaling: 04920, (ii) aminoacyl-tRNA biosynthesis: 00970, (iii) insulin signaling: 04910, (iv) OXPHOS system: 00190 and (v) ribosome: 03010 (Figure 2). Thus, there is a shared energy homeostasis impairment and protein and transcript processing alteration in mice and humans.

q-PCR validation of candidate genes belonging to dysregulated pathways

To validate the pathways commonly dysregulated in *Abcd1⁻* mice and human X-ALD, we analyzed the transcript contents of related genes with quantitative real-time PCR (qRT-PCR). We measured gene expression of 3–4 candidate genes per pathway in *Abcd1⁻* mouse spinal cords at the three ages under study as follows:

(1) Adipocytokine signaling: *Tnfrsf1a* (tumor necrosis factor receptor superfamily member 1A), *Ikbkb* (inhibitor of nuclear factor kappa-B kinase subunit beta), *NF-κB2* (nuclear factor NF-kappa-B p100 subunit) and *Adipor1* (adiponectin receptor 1).

(2) Aminoacyl-tRNA biosynthesis pathway: *Aars* (alanyl-tRNA synthetase), *Gars* (glycyl-tRNA synthetase) and *Sars* (seryl-tRNA synthetase).

(3) Insulin signaling: *Irs1*, *Irs2* (insulin receptor substrates 1 and 2) and *Akt2* (RAC-beta serine/threonine-protein kinase), which is a downstream effector of the insulin signaling pathway.

(4) Oxidative phosphorylation: *Ndufs7* [nicotinamide adenine dinucleotide (NADH) dehydrogenase (ubiquinone) Fe-S protein 7], *Sdha* (succinate dehydrogenase complex, subunit A), *Uqcrc1* (ubiquinol-cytochrome *c* reductase
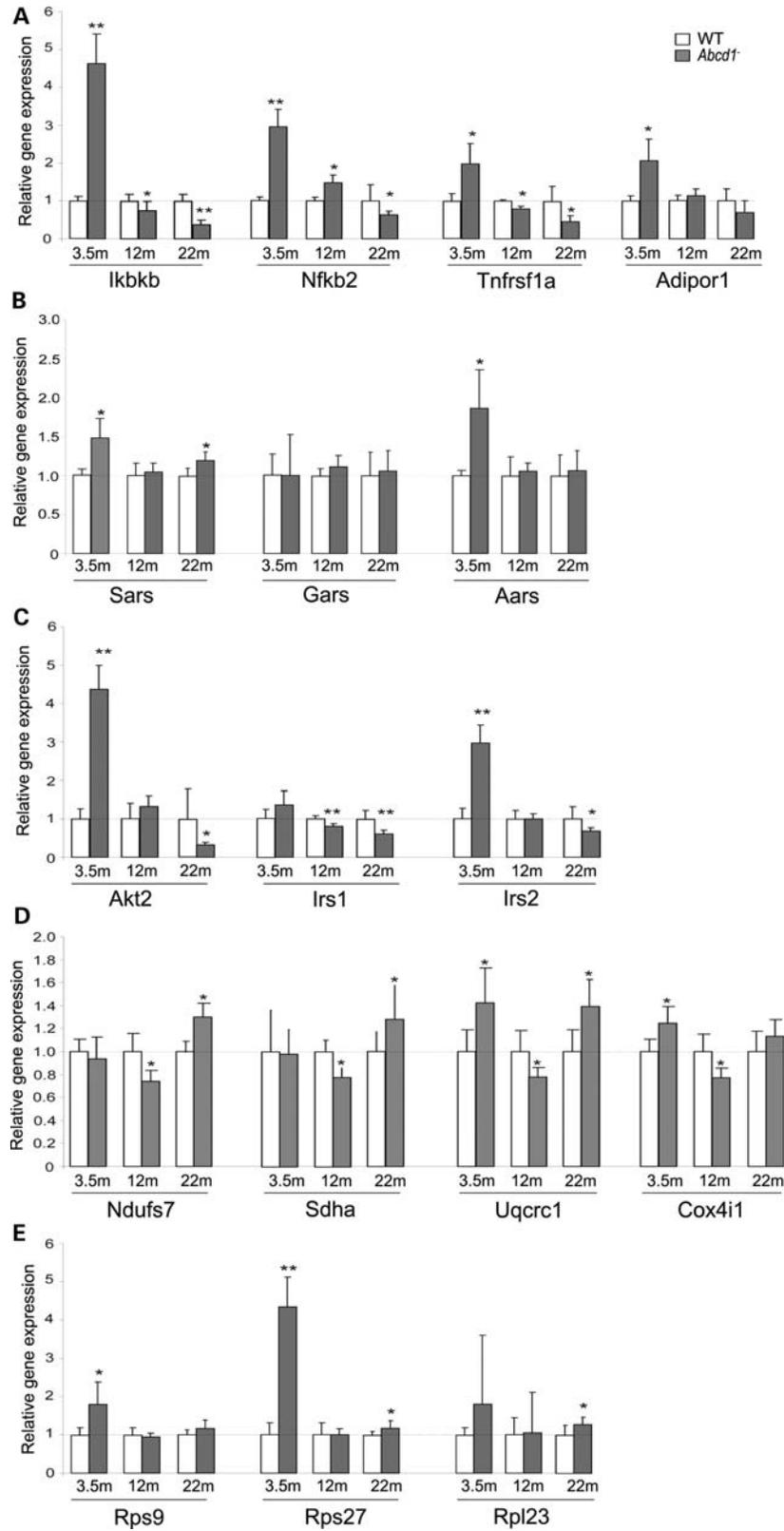
Figure 3. Validation of dysregulated pathways at three different ages in *Abcd1⁻* mice spinal cords. qRT-PCR measurements of (**A**) adipocytokine signaling pathway, (**B**) aminoacyl-tRNA biosynthesis, (**C**) insulin signaling pathway, (**D**) oxidative phosphorylation and (**E**) ribosomal subunits. *Ikbkb*, *NF-κB2*, *Tnfrsf1a*, *Adipor1*, *Sars*, *Gars*, *Aars*, *Akt2*, *Irs1*, *Irs2*, *Ndufs7*, *Sdha*, *Uqcrc1*, *Cox4i1*, *Rps9*, *Rps27* and *Rpl23* mRNA has been quantified by qRT-PCR. 18S was used as an internal control. Significant differences have been determined by Student's *t*-test. Significant differences are shown as $^*P < 0.05$ and $^{**}P < 0.01$.
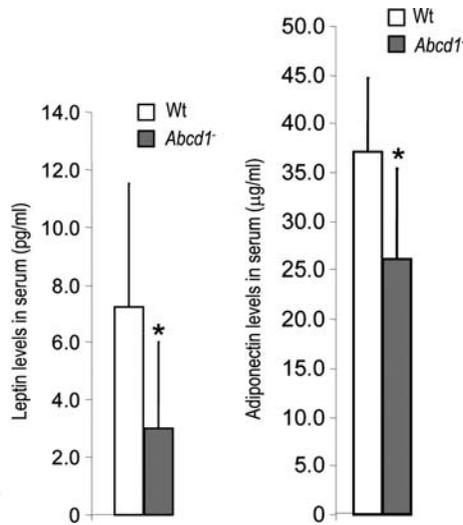
Figure 4. Leptin concentration was lower in serum from *Abcd1⁻* mice (**A**). Leptin (pg/ml) was measured in serum from 12-month-old Wt (*n* = 8) and *Abcd1⁻* (*n* = 9) mice. Adiponectin concentration was also lower in serum from *Abcd1⁻* mice (**B**). Adiponectin (μg/ml) was measured in serum from 12-month-old Wt (*n* = 10) and *Abcd1⁻* mice (*n* = 12). Statistical analysis was done by Student's *t*-test: *P < 0.05.

core protein I) and *Cox4i1* (cytochrome *c* oxidase subunit IV isoform 1).

(5) Ribosome: *Rps9* (ribosomal protein S9), *Rps27* (ribosomal protein S27) and *Rpl23* (ribosomal protein L23).

We found the differential expression of *Ikbkb*, *NF-κB2*, *Tnfrsf1a*, *Adipor1*, *Aars*, *Sars*, *Akt2*, *Irs1*, *Irs2*, *Ndufs7*, *Sdha*, *Uqcrc1*, *Cox4i1*, *Rps9*, *Rps27* and *Rpl23* (Figure 3).

The adipocytokines leptin and adiponectin were decreased in *Abcd1⁻* mice

We next aimed at gaining further insights into adipocyte-related dysregulation by measuring contents of leptin and adiponectin, which are the most abundant adipocytokines produced by adipocytes. We found that both leptin and adiponectin were reduced in serum of *Abcd1⁻* mice at 12 months of age with respect to controls (Figure 4). Remarkably, adiponectin is the only adipocyte-specific protein that is known to be negatively regulated by obesity and to show insulin-sensitizing properties with strong negative correlations with multiple indices of insulin resistance (16). This, together with the lower levels of adiponectin in *Abcd1⁻* mice, argues in favor of a metabolic abnormality in X-ALD.

Insulin desensitization in *Abcd1⁻* mice spinal cords

To further investigate the insulin signaling pathway, we examined the protein contents and phospho-activation of enzymes belonging to this pathway including IRS1, AKT, S6K and JNK in *Abcd1⁻* mouse spinal cords at 12 months of age (Figure 5A). Among other substrates, insulin stimulates the phosphorylation in tyrosine of IRS proteins, the phosphorylation of which mediates insulin action and is often attenuated in systemic insulin resistance, both in animal models and
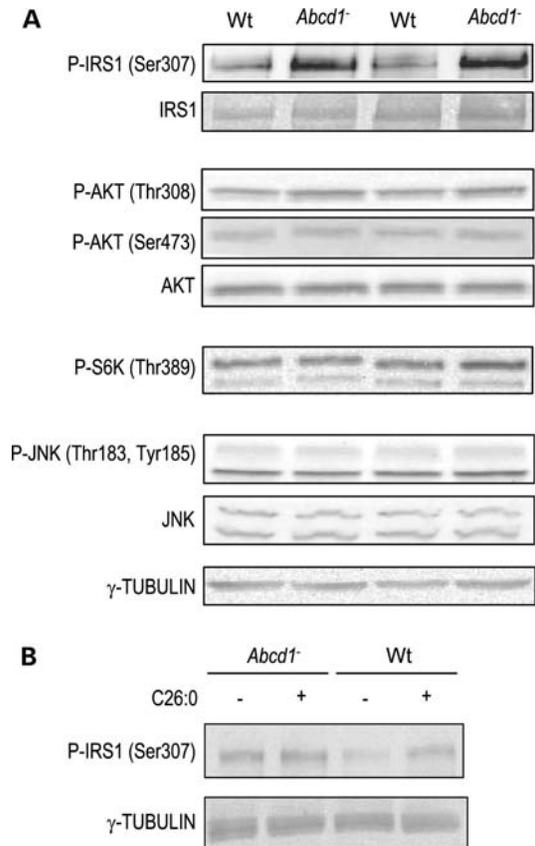

Figure 5. (**A**) Insulin signaling pathway in Wt and *Abcd1⁻* mouse spinal cords at 12 months of age. Western blots to monitor contents of IRS1, p-IRS1 Ser307, AKT, p-AKT Thr308, Ser473, p-S6K Thr389, JNK and p-JNK Thr183 and Tyr185 have been performed in whole spinal cord lysates from Wt and *Abcd1⁻* mice (*n* = 6 individuals per genotype). Representative blots are shown. Statistical analysis was done by Student's *t*-test: *P < 0.05. The phosphorylation of IRS1 in Ser307 was induced in *Abcd1⁻* mice spinal cord in the absence of insulin signaling activation, as shown by the lack of activation of kinases pS6K and JNK. (**B**) Phosphorylation of IRS1 ser307 in organotypic spinal cord slice culture (OSCSC). Western blots to monitor phosphorylation levels of IRS1 ser 307 have been performed on whole protein extracts from OSCSC (*n* = 6 cultures per genotype, *Abcd1⁻* or Wt littermates) incubated 24 h with BSA-conjugated C26:0 50 μM or BSA alone as control. Representative western blots are shown. C26:0 induces the IRS1 Ser307 phosphorylation in Wt but not *Abcd1⁻*-derived OSCSC.

human disease (for a review, see 17). We found no difference between genotypes regarding IRS1 tyrosine phosphorylation (data not shown) and the downstream effector AKT in Thr308 and Ser473 phosphorylation, arguing against activation of the insulin pathway associated to the disease. Alternatively, the phosphorylation of IRS1 in serine residues has been proposed as a general mechanism of functional inhibition of the IRS1 protein and, in particular, phosphorylation in Ser307 has become a molecular indicator of insulin resistance (18,19). To investigate whether *Abcd1⁻* mice manifest insulin desensitization, we measured levels of IRS1 Ser307 phosphorylation in *Abcd1⁻* mouse spinal cords at 12 months of age (Figure 5A). Our results provide evidence that Ser307 phosphorylation was induced in *Abcd1⁻* compared with wild-type (Wt) mice, suggesting reduced insulin sensitization in X-ALD pathology.
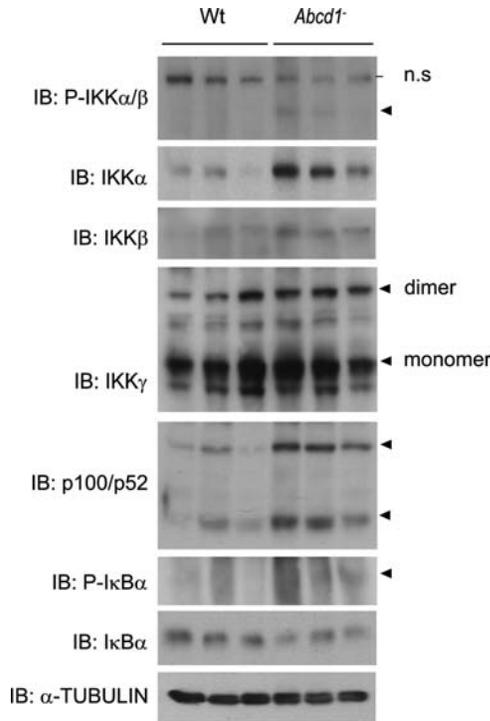
Figure 6. Activation of kinases IKK in mouse spinal cord (SC) at 12 months of age. Western blots to monitor levels of IKKα, IKKβ, IKKγ, NF-κB2 (p100/p52) and IκBα were performed in whole spinal cord lysates from Wt and *Abcd1⁻* mice (*n* = 6 individuals per genotype). Activated IKKs phosphorylate IκBα that liberates the NF-κB complex, which subsequently translocates into the nucleus.

VLCFA is a causative factor of insulin desensitization

Fatty acids (FAs) can mediate insulin desensitization associated with the phosphorylation of IRS1 on serine 307 (17,20,21). Because X-ALD pathology shows an accumulation of VLCFAs, it seemed likely that the FAs caused insulin desensitization. Hexacosanoic acid (C26:0) is the major VLCFA accumulated in X-ALD and can perturb the physiological properties of membranes, and it has been demonstrated to exert toxic effects in rat primary neuronal cell cultures and human fibroblasts (22,23). We evaluated the effect of C26:0 (10–100 μM, a 24-h incubation) on IRS1 phosphorylation in serine 307 using organotypic slice cultures of spinal cord (OSCSC). In OSCSC from Wt mice, 50 μM C26:0 induced an increase in IRS1 Ser307 phosphorylation, thus confirming our hypothesis that VLCFAs may trigger insulin desensitization (Figure 5B). In contrast, the *Abcd1⁻* OSCSC did not respond to C26:0 treatments, even at the higher dose of 100 μM. This suggests that IRS1 phosphorylation in these slices cannot increase over the sustained phosphorylation found in basal conditions, which largely exceed that of control slices.

IKK-mediated insulin desensitization in *Abcd1⁻* mice

It has been reported that S6K, JNK and IKKβ inhibit insulin actions by phosphorylating IRS1 on serine (18,19,21). Control over insulin signaling is achieved by an autoregulatory feedback loop whereby S6K, a downstream effector of mTOR, inhibits upstream elements, a process known as homologous desensitization. Findings in *S6k⁻* mouse model suggest that nutrient-induced S6K activation acts to suppress insulin signaling through modulating IRS1 Ser307 and Ser636/639 phosphorylation (21). Alternatively, mounting evidence indicates that activation of JNK is central to the development of insulin resistance in response to obesity mediated by fatty acid excess, by phosphorylating IRS1 in serine (for a review, see 17). To address whether S6K or JNK can induce insulin desensitization in *Abcd1⁻* mice at 12 months of age, we examined the activation status of S6K and JNK in Wt and Abcd1 knockout mice by western blot with specific anti-phospho-antibodies (that recognize P-Thr389 in the case of S6K and P-Thr183 and P-Tyr185 for JNK). We did not find any change in the activation of S6K or JNK in Abcd1 knockout mice (Figure 5A), suggesting that these kinases do not contribute to the phosphorylation of IRS1 Ser307 and, subsequently, to the insulin desensitization. Alternatively, we also examined IKK activation in our model. Our results show that total levels of IKKα, IKKβ and IKKγ (the three components of the IKK complex) are consistently increased in Abcd1 knockout mice compared with control mice. We also found detectable levels of active IKK specifically in the mutant animals, as measured with an antibody that recognizes both phosphorylated IKKα and IKKβ (Figure 6). To further confirm that this phosphorylated IKK found in the *Abcd1⁻* mice was active, we examined by western blotting the levels of total and phosphorylated IκBα protein, which is the main target of this kinase complex. Our results demonstrate that mutant mice show a slight but significant reduction in the total IκBα protein levels accompanied by increase IκBα phosphorylation, indicative of the activation of canonical IKK complex. These results also indicate that IKK is a good candidate to mediate phosphorylation of IRS1 in Abcd1 knockout mice.

TLR/NF-κB2 pathway was induced in *Abcd1⁻* mice

TLRs are a family of pattern-recognition receptors that play a critical role in the innate immune system by activating proinflammatory signaling pathways such as the NF-κB through IKK activation in response, for instance, to microbial pathogens. In our microarray analysis, we found that different elements of the TLR pathway were dysregulated in our mouse model at all ages under study. Similarly, adult X-ALD patients showed increased expression of the TLR2 (1.3-fold, *P* < 0.001) and the TLR4 coreceptor CD14 (4.5-fold, *P* < 0.001). These findings are in agreement with activation of the IKK complex in Abcd1 knockout mice. Moreover, microarray analysis demonstrated that *Nfkb2*, a well-characterized target of the NF-κB pathway, was upregulated in *Abcd1⁻* mice at 3.5 and 12 months and downregulated at 22 months of age, which was further confirmed by qRT-PCR (Figure 3). By western blot analysis, we demonstrated that p100 (the product of the *Nfkb2* gene) protein levels were significantly increased in mutant mice compared with the controls. Most importantly, not only p100 levels, but also the amounts of its active form p52 (involved in the non-canonical NF-κB signaling), were significantly upregulated in *Abcd1⁻* spinal cords at 12 months of age (Figure 6). Together, these results indicate
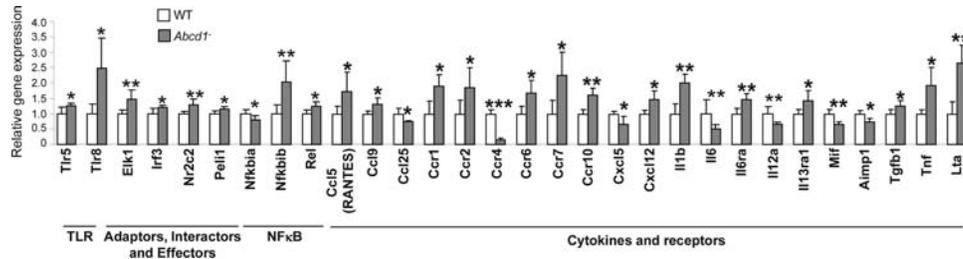
Figure 7. Activation of TLR/NF-κB in mouse spinal cords at 12 months of age. A q-PCR was performed to measure a gene array including TLRs, TLR adaptors, NF-κB forms, several cytokines and their receptors. Only differentially expressed genes are shown (*n* = 6 individuals per genotype). The data point to a general activation of TLR/NF-κB pathways, wherein we highlight the upregulation of *Tlr8, Tlr5, Nfkbib*, RANTES (*Ccl5*), *Ccr1, Ccr2, Ccr7, Il1b, Tnf* and *Lta*. Significant differences have been determined by Student's *t*-test: *$P < 0.05$, **$P < 0.01$ and ***$P < 0.001$.

that both canonical and non-canonical NF-κB pathways are active in Abcd1 knockout mice and suggest a TLR-mediated induction of the IKK complex leading to gene transcription of proinflammatory cytokines. To substantiate our microarray findings, we used a qRT-PCR array (SABioscience) to measure expression of TLRs, NF-κB genes, several cytokines and their receptors at 12 months of age in the Abcd1 null mice. TLRs such as *Tlr5* and *Tlr8*, together with some of their adaptors, interactors or effectors (*Elk1, Irf3, Nr2c2* and *Peli1*) were induced in Abcd1 null mice (Figure 7). Activation of NF-κB was confirmed by inductions of its messenger and further by induction of its target proinflammatory cytokines RANTES (*Ccl5*), *Tnf* and *Il1b* (Figure 7).

Oxidative stress underlying disease progression

Previous studies from our laboratory demonstrate that oxidative stress contributes to the progression of X-ALD (11,22,24,25). To compare our transcriptomic data with the knowledge derived from functional studies in the field, as a means of reverse validation, and in the absence in KEGG of pathways encompassing all enzymatic and signaling stress-related pathways, we directly assessed whether differentially expressed data, as detected by GSEA analysis in *Abcd1⁻* mice, were enriched in genes involved in oxidative stress. First, we created a gene list by retrieving genes related to oxidative stress from the literature, text mining and manually curated data (407 genes; see Supplementary Material, Figure S5). We then compared this list against our differential data and found that the selected genes were more frequently differentially expressed in mice at all ages than it would be expected by random with a *P*-value of <0.001. This confirms that oxidative stress in the spinal cord is a signature common to all ages that may contribute to ALD disease progression. Of note, mitochondria are a primary source generating the reactive oxygen species (ROS) superoxide (O_2^-) and thus may play a central role in *Abcd1⁻* ROS production. We observe that as a whole, the mitochondrial transcriptome is largely dysregulated (Figure 8). Several enzymes so far known to generate ROS are dysregulated (26). In particular, we identified the induction of the tricarboxylic acid (TCA), α-ketoglutarate dehydrogenase (dihydrolipoamide *S*-succinyltransferase—DLST) (27) or the respiratory chain, and the repression of the TCA enzymes oxoglutarate dehydrogenase (OGDH)) and the aconitase 2 (ACO) at 3.5 months of age, as depicted in Figure 8. Moreover, the

antioxidant defence system to detoxify the ROS seems to be differentially dysregulated. Enzymatic components induced in *Abcd1⁻* spinal cords include glutathione peroxidases (GPX), phospholipid hydroperoxide glutathione peroxidase (PGPX), several glutathione *S*-transferases (GSTs), peroxiredoxins (PRX), glutaredoxins (GRX) and thioredoxins (TRX). In addition, the glutathione synthesis seems to be impaired because the expression of the key enzymes glutamate-cysteine ligase catalytic subunit (GCLC) and glutathione synthetase (GSS) are repressed (see Supplementary Material, Figure S6 for expression values at 3.5 months of age). The observed induction of the enzymatic glutathione antioxidant system that consumes the reduced GSH, together with the repression of GSH biosynthesis, lends support to a GSH depletion scenario, which commonly occurs during oxidative stress situations. This has been experimentally verified in (24). Of note, the predicted mitochondrial dysfunction and dysregulation of calcium signaling as depicted in Figure 8 is in agreement with the effects observed in primary neural cells challenged with excess of VLCFAs (23).

An integrative depiction of the validated pathways and their cross-talk is shown in Figure 9. These data should serve as a platform for an improved understanding of physiopathogenesis and thus for rational therapeutic design against this dreadful disease.

DISCUSSION

We have identified the main metabolic and cell signaling pathways playing a potential role in X-ALD pathogenesis based on a functional-enrichment analysis of transcriptomic data from *Abcd1⁻* mice and human X-ALD patients. Mice and humans share a signature that encompasses mitochondrial dysregulation, ROS production with antioxidant defense impairment, insulin and adipocytokine signaling dysregulation, protein synthesis and turnover dysregulation and an NF-κB mediated proinflammatory response amplified by the activation of the TLRs. A most relevant finding is that pathway dysregulation was detected in the mice as early as 3.5 months, more than a year before the first neurological symptoms appears, and in human brain samples from regions not affected by the disease yet. We thus conclude that the dysregulated pathways may contribute to the X-ALD disease and VLCFA excess might act as a first causative factor of the cellular mechanism underlying X-ALD pathology. The mechanisms by which
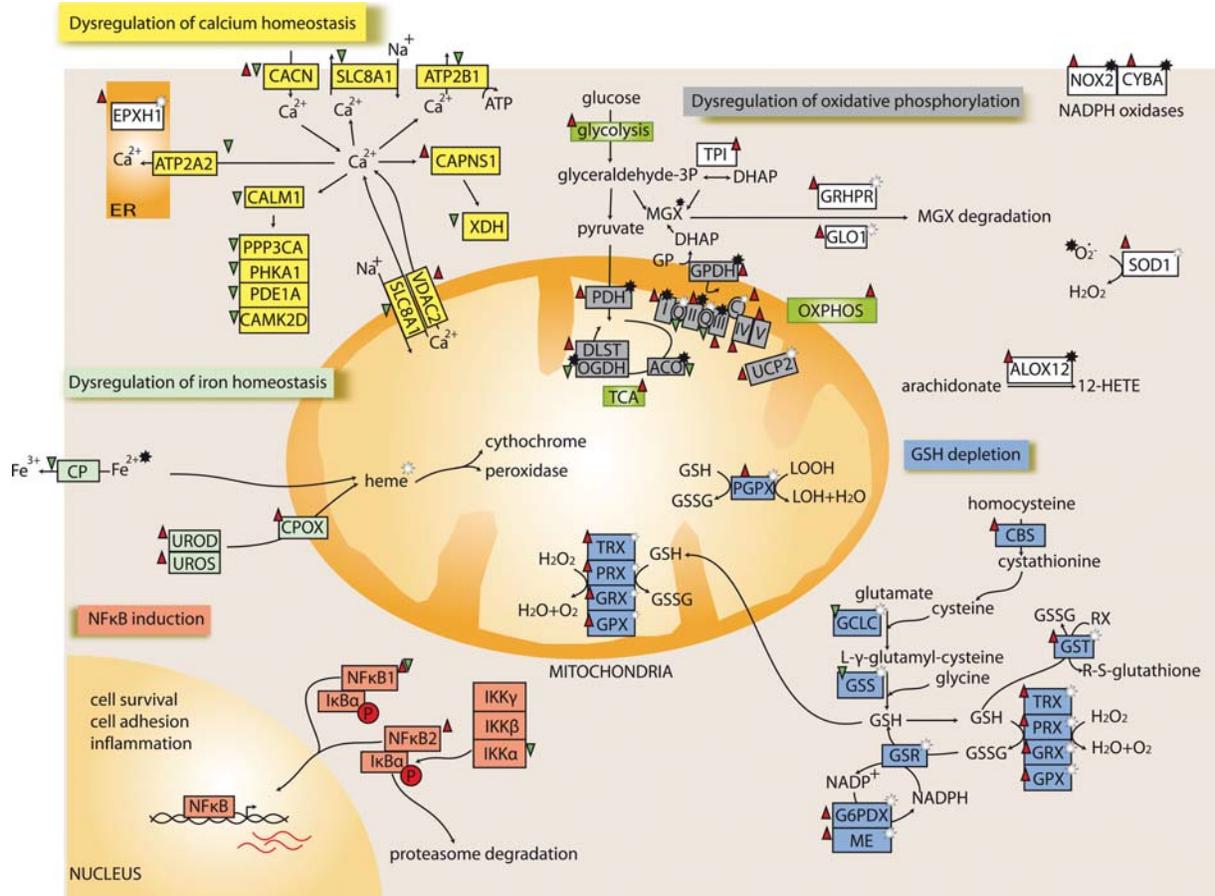
Figure 8. The role of oxidative stress in ALD progression in spinal cord is already manifesting as early as 3.5 months of age. The picture shows dysregulated gene expression, induced (red triangle) and repressed (green triangle), of processes and components involved in ROS generation (black stars) and antioxidant defense (white stars). Perturbations in oxidative phosphorylation, iron and calcium homeostasis and changes in GSH homeostasis may altogether represent causes and consequences of increased oxidative stress. ROS might activate NF-κB leading to the regulation of genes involved in cell survival and inflammation. 12-Hydroxyeicosatetrenoate (12-HETE), arachidonate 12-lipoxygenase (ALOX12), ATPase, Ca^{2+} transporting, cardiac muscle, slow twitch 2 (ATP2A2), ATPase, Ca^{2+} transporting, plasma membrane 1 (ATP2B1), calcium-channel, voltage-dependent, alpha 2/delta subunit 3 (CACNA2D3), calcium-channel, voltage-dependent, gamma subunit 5 (CACNG5), calcium-channel, voltage-dependent, L-type, alpha 1D subunit (CACNA1D), calcium/calmodulin-dependent protein kinase (CaM kinase) II delta (CAMK2D), calmodulin 1 (CALM1), protein phosphatase 3, catalytic subunit, alpha isoform (PPP3CA), ceruloplasmin (CP), coenzyme Q10 (CQ), coproporphyrinogen oxidase (CPOX), cystathionine beta-synthase (CBS), cytochrome *b*-245 (CYBA), cytochrome *c* (CytC), DLST, dihydroxyacetone-phosphate (DHAP), electron transport chain complexes I:V (C-I:C-V), epoxide hydrolase 1, microsomal (EPHX1), glucose-6-phosphate dehydrogenase X-linked (G6PDH), GCLC, GRX, GSH, glutathione disulfide (GSSG), GPX, glutathione reductase (GSR), GST, GSS, glyceraldehyde-3-phosphate (G3P), glycerol-3-phosphate dehydrogenase (GPDH), glyoxalase 1 (GLO1), glyoxylate reductase/hydroxypyruvate reductase (GRHPR), nuclear factor of kappa light polypeptide gene enhancer in B-cells inhibitor alpha (NFKBIA or IκBα), conserved helix−loop−helix ubiquitous kinase (CHUK or IKKα), inhibitor of kappa light polypeptide gene enhancer in B-cells, kinase beta (IKBKB or IKKβ), inhibitor of kappa light polypeptide gene enhancer in B-cells, kinase gamma (IKBKG or IKKγ), lipid hydroperoxide (LOOH), lipid hydroxide (LOH), malic enzyme (ME), NADPH oxidase 1 (NOX1), nuclear factor of kappa light polypeptide gene enhancer in B-cells 1 and 2 (NF-κB1 and NF-κB2), OGDH, PRX, phosphodiesterase 1A, calmodulin-dependent (PDE1A), PGPX, phosphorylase kinase, alpha 1 (PHKA1), pyruvate dehydrogenase (PDH), solute carrier family 8 (sodium/calcium exchanger), member 1 (SLC8A1), thioredoxin (TRX), TCA, triosephosphate isomerase 1 (TPI), uncoupling protein 2 (UCP2), uroporphyrinogen decarboxylase (UROD), uroporphyrinogen III synthase (UROS).

excess of FA induce metabolic impairment, mitochondrial dysfunction, insulin resistance and immune responses are traditionally studied in classical metabolic organs such as liver, adipose or muscle tissues, whereas their role in CNS has seldom been addressed. X-ALD constitutes a bona fide model in which to study the impact of VLCFA accumulation in the CNS, as well as in the adrenal cortex. Our results may help to decipher the cellular mechanisms contributing to X-ALD pathology with positive implications for therapy. A working model hypothesis is depicted in Figure 9. Below the main tenets are discussed.

VLCFAs cause oxidative stress and mitochondrial dysregulation

We have proposed that VLCFA-mediated oxidative stress is a causative agent in X-ALD physiopathogenesis. We have previously shown signs of oxidative damage in spinal cords from the *Abcd1*-null mice and in fibroblasts from X-ALD patients, with oxidative, glycoxidative and lipoxidative damage to proteins and altered expression levels of enzymatic antioxidant defences such as glutathione peroxidase 1 (GPX1) and superoxide dismutases 1 and 2 (22). Second, we have
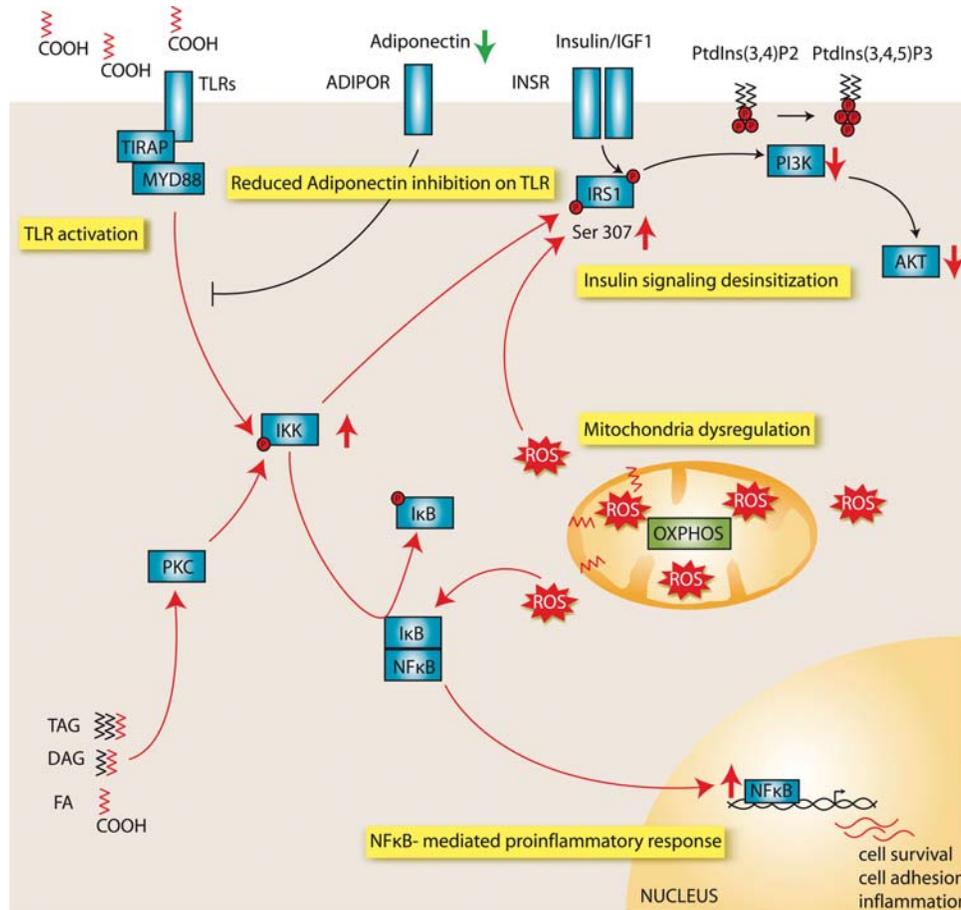
Figure 9. Proposed model for X-ALD disease mechanism. Taking together our functional validation that ensued our transcriptomic data mining and the experimental evidence provided, we put forth the following model: disease progression appears mediated by the successive action of a primarily VLCFA excess, mitochondrial dysregulation combined with ROS production and antioxidant defenses depletion, insulin desensitization, TLR activation and NF-κB-mediated proinflammatory response. The increased lipid load induces a stress response leading to the production of ROS contributing all together to a mitochondrial dysregulation. The activation of IKKs links VLCFA-induced metabolic deficiency with an NF-κB-mediated proinflammatory response. IKK activation desensitizes insulin signaling via phosphorylation of IRS1 on serines. Insulin controls glucose uptake through tyrosine phosphorylation of insulin receptor substrate (IRS) proteins. Activation of phosphatidylinositol 3-kinase (PI3K) and generation of phosphatidylinositol-3,4,5-trisphosphate (PtdIns(3,4,5)P3) activates AKT. But IRS1 serine phosphorylation attenuates insulin sensitivity and subsequently decreases glucose uptake and insulin-induced metabolism. IKKs can be induced by FA via the activation of TLRs and PKC, and the latter can be activated by DAG. The low levels of adiponectin might contribute to the increased proinflammatory response in X-ALD by reducing the inhibitory adiponectin effect on TLR signaling.

recently found out that oxidative damage specifically affects five key enzymes of glycolysis and TCA cycle in *Abcd1*⁻ mice and human X-ALD fibroblasts. Third, NADH and adenosine triphosphate (ATP) levels are significantly diminished in these samples, together with decrease in pyruvate kinase activities and GSH levels, and increase in NADPH (24). Fourth, anti-oxidant treatment largely erases signs of oxidative damage and halts axonal degeneration and disability of *Abcd1* null mice (25). Finally, a wide array of mitochondrial genes related to the pyruvate and OGDH complexes, TCA cycle, OXPHOS system and different organelle antioxidant defenses are dysregulated according to previous (22,24) and present transcriptome data (see Figure 8). There is also immunohistochemical evidence of oxidative stress and damage in brains from cALD and cAMN patients, mainly resulting from lipid peroxidation, and mostly occurring in the

inflammatory demyelinated lesions, as well as in adrenal cortex (28,29). The accumulation of excess lipid, in particular, saturated FA, may damage cells by causing stress on membranes of lipid-metabolizing organelles, especially mitochondria. In particular, VLCFAs are found as lateral chains of complex lipids, such as phosphatidylcholine and phosphatidylethanolamine, thus playing a main structural role as components of cellular membranes (30–32). We propose that VLCFAs in the mitochondrial membranes might induce a stress response leading to the production of ROS and oxidation of main protein components of Krebs cycle contributing all together to a mitochondrial dysregulation, sinking of ATP levels and the collapse of energy homeostasis (24). Our transcriptomic analysis aligns with previous experimental data showing the impaired energy production and dysregulated organelle antioxidant defenses (11,22,24,25).

VLCFAs cause desensitization of insulin signaling via IKK

Our findings point to IKK-mediated insulin desensitization in X-ALD. IRS1 serine phosphorylation attenuates insulin sensitivity and subsequently decreases glucose uptake and insulin-induced metabolism. Indeed, IRS1 serine phosphorylation seems to be associated with increased free fatty acids levels since IRS1 Ser307 phosphorylation has been induced in muscle, white adipose tissue and liver tissues of mice fed a high-fat diet (20,21). Although the phosphorylation of IRS1 Ser307 has been associated to insulin resistance (18,19), the phosphorylation of IRS1 Ser307 observed in spinal cords of *Abcd1⁻* mice points to insulin desensitization but not resistance, because an intraperitoneal glucose tolerance test has repeatedly shown no differences between genotypes (Supplementary Material, Figure S7). IRS1 Ser307 is reported to be a phosphoacceptor of S6K, JNK and IKK (18,19,21). Our findings point out IKK-mediated IRS1 phosphorylation in Ser307 in X-ALD. A direct link between FA and IKK activation has formerly been proposed with the accumulation of intracellular fatty acyl-CoA and diacylglycerol (DAG), which can activate protein kinase C (PKC) θ in muscles or PKCδ in the liver (33,34), which in turn activate IKK contributing to insulin resistance (17). In addition, the chronic production of ROS species due to excess of VLCFAs (22) can lead to abnormal changes in intracellular signaling and result also in insulin resistance via phosphorylation of IRS proteins by stress-sensitive kinases such as IKKβ (35).

TLR/NF-κB2 pathway stimulates a proinflammatory phenotype via IKK

We demonstrated that the product of the NF-κB gene, p100 and its active form p52, was significantly upregulated in *Abcd1⁻* mice spinal cords. These results, together with the IKK complex induction, indicate that NF-κB pathway is active in Abcd1 knockout mice leading to gene transcription of proinflammatory cytokines such as RANTES (CCL5), TNF and IL-1β. Of note, our data are in agreement with a previous report, which established a link between VLCFA accumulation and inflammation in astrocytes. Inactivation of *Abcd1* and *Abcd2* genes induced an inflammatory response mediated by transcription factors NF-κB, AP-1 and C/EBP (36). TLRs are a family of pattern-recognition receptors that play a critical role in the innate immune system by activating proinflammatory signaling pathways such as the NF-κB through IKK activation in response to microbial pathogens. Our microarray analysis indicates that different elements of the TLR pathway were dysregulated in our mouse model and, in particular, showed altered expression of TLR2 and the TLR4 coreceptor CD14 in cAMN patients as in other neurodegenerative diseases (37,38). Indeed, there is an evolutionarily conserved overlapping of pathways that regulate metabolic and immune functions through common key regulatory molecules and signaling systems (39). This may allow nutrients such as FA to act through pathogen-sensing systems such as TLRs, giving rise to metabolically or nutritionally induced inflammatory responses (20,40). It is worth mentioning that, like macrophages, microglial cells express TLRs, respond to TLR ligands and produce proinflammatory

mediators. This is highly relevant to X-ALD pathology because microglial cells are thought to be the main type of the innate immune system in the nervous tissue and able, when replaced by hematopoietic stem-cell transplantation or gene therapy, to arrest inflammatory demyelination (41). It is tempting to speculate that the VLCFAs accumulated due to *Abcd1* inactivation could activate TLR signaling leading to NF-κB-induced proinflammatory response in X-ALD with the subsequent activation of RANTES (CCL5), TNF and IL-1β as shown. In fact, both histologically normal-appearing areas as well as inflammatory areas of childhood ALD brains show increased levels of proinflammatory cytokines TNF, IL-1β, IL-6 and IL-2, indicating a primary relationship between the metabolic abnormality and inflammation in the disease progression (42).

Downregulation of adiponectin contributes to the proinflammatory state

We have detected lower levels of adiponectin and leptin in X-ALD mice. Adipocyte-derived adipocytokines are key molecules linking metabolism and inflammatory response. It is tempting to speculate that the VLCFAs and/or other lipid metabolites accumulated due to the Abcd1-transporter inactivation might reduce the levels of adiponectin contributing to the increased proinflammatory response in X-ALD. Unlike leptin and TNF, adiponectin has an anti-inflammatory effect as shown by the capacity to suppress the synthesis of TNF in endothelial cells and to induce the production of anti-inflammatory cytokines such as IL-10 and IL-1 receptor antagonist (IL-1RA) in human monocytes, macrophages and dendritic cells (16,43). In addition, adiponectin suppresses TLR-induced NF-κB activation in macrophages (44). Therefore, the lower levels of adiponectin in *Abcd1* null mice might account for a compromised anti-inflammatory reaction to counteract NF-κB-mediated inflammatory response induced by TLR signaling.

In contrast to leptin, adiponectin does not cross the blood–brain barrier in mice and is not detectable in human cerebrospinal fluid. However, we detected overexpression of the adiponectin receptor *Adipor1* in spinal cords of *Abcd1⁻* mice by qRT-PCR. In agreement with these findings, it has been demonstrated expression of adiponectin receptors in brain endothelium and the reduction of IL-6 secretion in brain endothelial cells upon treatment with adiponectin (45).

Is inflammation in X-ALD good or bad?

Having demonstrated that a proinflammatory reaction lurks in X-ALD prior to the development of axonopathy, in the case of the mouse model with an AMN-like phenotype, or aberrant microglia activation and demyelination, in the case of cAMN and cALD patients, the question arises whether this early inflammation contributes or not to the ensuing tissue damage. In general, the role of the immune system in neurodegeneration is still highly debated. It has been demonstrated that acute TLR activation via lipopolysaccharide administration regulates processes required to efficiently eliminate cell debris and promote repair in the brain. These events increase the recruitment of oligodendrocyte progenitor cells, favor

remyelination and confer neuroprotection. But without the rapid clearance of myelin debris or toxic elements from the brain, microglial cells can react differentially and mount a proinflammatory response that is detrimental for neurons and astroglia, resulting in demyelination, synaptic dysfunction and ultimately neurodegeneration (46). There is an increasing body of evidence in support that TLR signaling mediates activation of microglia and the release of proinflammatory molecules leading to neurotoxic processes in the course of various CNS diseases. For instance, neurotoxic effects of TLR activation have been observed in specific regions of the brain during chronic conditions such as in Alzheimer's disease where Aβ fibrils bind to CD14 and activate microglia (47) and anti-CD14 strategies reduce the Aβ-stimulated microglia neurotoxicity (48). Thus, the TLR-induced activation of microglia in nervous tissue depends on a subtle balance between beneficial and harmful effects and the long-term consequences of such TLR activation, in particular, in X-ALD, have yet to be investigated. Future studies in mice using pharmacological inhibitors to suppress NF-κB activation (e.g. salicylates that inhibit IKKβ (49) or treatment with adiponectin to block TLR pathways) will shed light on whether the early proinflammatory phase of X-ALD is neuroprotective or, in the contrary, contributes to axonopathy. In the latter case, an anti-inflammatory regime should complement the antioxidant therapies that have proven successful in the *Abcd1*⁻ mice (25).

Whatever the role of inflammation in the adult axonopathy, an inevitable question is whether a connection between the pre-symptomatic inflammation and the robust, deadly inflammation in cAMN and cALD exists. A key idea is that activation of microglia to highly deleterious states depends on the sequential appearance of at least two hits, the first one rendering microglia mildly activated, thus priming its response to ensuing hits. A precedent for this scenario exists in Alzheimer's disease animal models, wherein it has been shown that systemic inflammation-mediated increase of Fc receptors in microglia increases its reaction to Aβ (50). We thus posit that VLCFA-stimulated microglia in X-ALD may present a more robust response to a second stimulus of yet unknown nature, thus producing the switch from AMN to cAMN and cALD. In the absence of the second hit, the inflammatory reaction may proceed with its natural course and enter the repair- and phagocytosis-prone phase, where microglia is deactivated and produces anti-inflammatory cytokines. A resolution of the inflammatory process would explain why lack of inflammatory lesions has been reported in *post-mortem* tissues from AMN terminal patients leading to the widespread misconception hitherto that AMN, unlike cALD, is a non-inflammatory condition (4). Overall, the discovery of a dysregulated pathway signature common to *Abcd1*⁻ mice, cAMN and cALD points to the existence of a basal pathogenic mechanism in X-ALD leading to either AMN (or the AMN-like condition in the mouse) or to the cerebral forms in humans.

In conclusion, our analyses pave the way for the characterization of VLCFA-mediated inflammation in the CNS and the identification of immunomodulatory therapeutic targets to halt AMN progression and conversion into more severe forms. The results highlight, in any event, the existence of a metabolism-mediated inflammatory response that may provide insights into the X-ALD pathogenesis, but also into the progression of other neurodegenerative diseases featuring a link between FA excess and neuroinflammation.

MATERIALS AND METHODS

Mouse breeding

The generation and genotyping of *Abcd1*⁻/⁻ mice have been previously described (8,9,11,51). Mice used for microarray experiments were on a pure C57BL/6J background. Animals were sacrificed, and spinal cords were recovered and conserved at −80°C. Total RNA for microarrays analysis was extracted using RNeasy Kit (Qiagen, Valencia, CA, USA) from four animals at 3.5, three at 12, four at 22 months of age and 11 Wt, age-matched *Abcd1*⁻ spinal cords. All samples were hybridized in duplicate and analyzed in dye swap. All methods employed in this study are in accordance with the Guide for the Care and Use of Laboratory Animals published by the US National Institutes of Health (NIH Publications No. 85-23, revised 1996).

Custom cDNA microarray for X-ALD mouse

A cDNA microarray was manufactured at IGBMC (Institut de Génétique et de Biologie Moléculaire et Cellulaire). The array consisted of 20 736 mouse cDNA clones representing ~15 000 Unigene clusters. The clones were selected from public cDNA libraries, the NIA 15K (http://lgsun.grc.nia.nih.gov/cDNA/cDNA.html) and the IMAGE collection (http://image.llnl.gov/). Some clones were also acquired from a private cDNA library collection (C. Benoist, Joslin Diabetes Center, Boston, MA, USA). The cDNAs were amplified by PCR using vector-specific primers, purified using MultiScreen FB filter plates (Millipore, Billerica, MA, USA) and verified by gel electrophoresis. After dehydration, PCR products were resuspended in the spotting buffer (75% formamide and 25% water) and spotted in duplicate onto Ultra-GAPS™ amino-silane-coated slides (Corning BV, Schiphol-Rik, the Netherlands) using a MicroGrid II Arrayer (BioRobotics Ltd, Cambridge, UK). The printed slides were dried for 48 h and cross-linked by UV at 600 mJ/cm².

For probe synthesis in the dye swap experiments, total RNA (200 ng) was amplified by linear PCR and the amplification products were labeled with dUTP-Cy3 and dUTP-Cy5 by random priming (Bioprime, Invitrogen). Labeled cDNAs were purified using Nucleospin Extract II columns (Macherey Nagel, Düren, Germany) and hybridized in a Discovery station using ChipHybe 80 hybridization buffer at 42°C for 12 h without any final stringency washes (hybridization automate, reagents and microarray hybridization procedure are from Ventana Medical System, Tucson, AZ, USA).

Arrays were scanned using ScanArray 4000 (Packard Biochips, Billerica, MA, USA) and images quantified using Imagene 5.0 (BioDiscovery Microarray Bioinformatics Software, Marina Del Rey, CA, USA). Detailed information is available on the IGBMC microarray web site (http://www-microarrays.u-strasbg.fr) (52).

Human brain samples

Brain tissues from ALD patients and age-matched controls were obtained from the Brain and Tissue Bank for Developmental Disorders at the University of Maryland, Baltimore, MD, USA. Frozen blocks of normal-appearing white matter were dissected from frontal or parietal lobes from 20 controls and 21 ALD patients. All the children and adults with cerebral ALD had the conventional 'parieto-occipital' form of cerebral ALD. White matter sections of ALD patients and controls were stained with LFB to detect demyelination, demyelination edge and normal-looking area. Brain tissue sections were processed when two to three adjacent sections showed no sign of demyelination with LFB staining and no perivascular cuffs of lymphocytes using hematoxylin and eosin staining (6,15).

RNA isolation and microarray processing of human ALD samples

Total RNA was extracted from 41 frozen white matter samples (including some replicate samples from some donors) obtained from cALD (7 samples), child controls (8 samples), adult cAMN (14 samples) and adult controls (12 samples) using a Polytron type homogenizer (YellowLine DI 25 Basic) and TriZol reagent (Invitrogen, Paisley, UK) in a ratio of 1 ml of TriZol to 20 mg of tissue. RNA was further purified using RNeasy mini-columns (Qiagen, Valencia, CA, USA) including on-column DNAse-1 step and elution in water. The quantity of extracted RNA was determined by spectrophotometry, and quality was assessed using an Agilent 2100 Bioanalyzer (South Plainfield, NJ, USA). Insufficient RNA yield was achieved for seven samples, which were not progressed to the microarray analysis. For the remaining 34 samples, 7 µg of total RNA was processed to Biotin-labeled cRNA and hybridized to HG-U133A GeneChips in accordance with the Affymetrix protocol (Affymetrix, Santa Clara, CA, USA). Arrays were scanned on a GeneChip Scanner 3000, and fluorescence intensity for each feature of the array was obtained by using GeneChip Operating Software (Affymetrix). Following standard MAS5.0 Affymetrix quality control criteria, five samples failed quality control (β-actin $3'/5'$ ratios > 4), four samples were identified as outliers using principal component analysis (representing probable grey matter contamination) and one file was lost during transfer. As a result, 24 samples were progressed into statistical analysis (3 cALD, 3 child controls, 8 cAMN and 10 adult controls) (Table 1).

Microarray data normalization and differential expression analysis

Pre-processing of raw data and statistical analyses were performed using Bioconductor packages in R programming environment (53) and custom software written in Perl. For mouse arrays, background correction was performed using the 'normexp' method implemented in the Bioconductor LIMMA package to adjust local median background estimates (54). Background-corrected intensity data were normalized using the Print-tip loess method to remove the bias within each array and the A-values quantile normalization (Aquantile) to remove the bias between arrays.

Table 1. Human sample characteristics

Type	Sexe	Age	Brain white matter area
cALD	Male	6	Frontal
cALD	Male	13	Frontal
cALD	Male	8	Frontal
cAMN	Male	17	Frontal
cAMN	Male	39	Frontal
cAMN	Male	43	Parietal
cAMN	Male	47	Frontal
cAMN	Male	28.5	Frontal
cAMN	Male	33	Frontal
cAMN	Male	48	Parietal
cAMN	Male	66.5	Frontal

To determine the target genes that are differentially express at 3.5, 12 and 22 months in ALD mouse spinal cords, *Abcd1⁻* and Wt profiles for each age were compared using statistical linear model in LIMMA. It was estimated the intra-spot correlation between the two channels by using the function 'intraspotCorrelation' and further the regression function 'lmscFit' fitted a linear model to the two-color data. To calculate differential expression, *P*-values were computed by empirical Bayes moderated *t*-statistics at a level of 0.05.

For human Affymetrix arrays, we read CEL files and then corrected background, summarized and normalized the data by robust microarray analysis method. Further, we estimated the fold change and standard errors by fitting a linear model (using the lmFit function) for each gene given the groups of arrays and then compute a moderated *t*-statistics of differential expression by applying empirical Bayes at a level of 0.05. We corrected *t*-test *P*-values for multiple hypotheses testing by calculating the false discovery rate ($P < 0.05$).

The microarray experiments have been deposited in the Array Express Database under accession numbers E-MTAB-79 and E-MEXP-3288.

Functional enrichment analysis

Enrichment analysis detects whether a certain GO term or KEGG pathway occurs more frequently in the set of genes than it would be expected based on the frequency of its occurrence in the entire Chip. The Chip spotted transcripts were annotated by Annbuilder package for getting GO terms, and by KEGG package and custom software written in Perl and R for pathway annotation. To evaluate which pathways or functional categories were enriched in ALD mice, we computed the Gene set enrichment analysis ('geneSetTest' function) and hypergeometric distribution test (GOHyperG and 'phyper' functions). We used $P < 0.05$ as the cutoff point to determine whether GO term or a KEGG pathway was significantly enriched.

GeneSetTest function from Limma package tests whether a set of genes is enriched for differential expression. Its principle is the same as for Gene Set Enrichment Analysis introduced by Mootha *et al*. (55), but the statistical tests used are different. It is based on a set of probe-wise *t*-statistics arising for microarray analysis. We have computed four different tests: (i) upregulated genes, with positive *t*-statistics, (ii) downregulated genes, with negative *t*-statistics, (iii) up- or

downregulated genes as a whole and (iv) genes differentially expressed regardless of the direction. When the function gives a significant result, it means that at least one of four tests is significant. GOstats package contains a function called GOHyperG that can be used to find GO terms that may be enriched in a subset of genes. It is based on a hypergeometric distribution. We used the 'phyper' hypergeometric distribution function from stats package to determine enriched KEGG pathways in a subset of genes.

Quantitative real-time PCR

One microgram of RNA was transcribed into cDNA using Superscript II reverse transcription reagents in a final volume of 25 μl (Invitrogen). A TaqMan RT-PCR was performed within the ABI PRISM 7300HT sequence detection system using the TaqMan Universal PCR master mix and the standardized primers for mouse *Ikbkb* (Mm01222247_m1), *Nfkb2* (Mm00479807_m1), *Tnfrsf1a* (Mm01182929_m1), *Adipor1* (Mm01291334_mH), *Sars* (Mm00803379_m1), *Gars* (Mm00619269_m1), *Aars* (Mm00507627_m1), *Akt2* (Mm00545827_m1), *Irs1* (Mm01278327_m1), *Irs2* (Mm03038438_m1), *Ndufs7* (Mm00503957_m1), *Sdha* (Mm01352366_m1), *Uqcrc1* (Mm00445911_m1), *Cox4i1* (Mm01250094_m1), *Rps9* (Mm00850060_s1), *Rps27* (Mm00850051_g1) and *Rpl23* (Mm00787512_s1).

Each sample was run in duplicate, and the mean value of the duplicate was used to calculate the mRNA expression of the genes of interest which were normalized to that of the reference control (18S, Hs99999901) using the comparative ($2^{-\Delta Ct}$) method, according to the manufacturer's instructions.

PCR array (TLR signaling pathway and inflammatory cytokines and receptors)

PCR microarray for TLR pathway was performed by using RT2-Profiler PCR Array from SuperArray Bioscience (Mouse Toll-Like Receptor Signalling Pathway PAMM-018 and Inflammatory Cytokines and Receptors PAMM-011). A 96-well plate contains gene-specific primer sets for 84 relevant genes for both TLR Signalling Pathway and Inflammatory Cytokines and Receptors, five housekeeping genes and two negative controls. After performing thermal cycling, real-time amplification data were analyzed by using ABI Prism 7300HT software. Gene expression was normalized to internal controls (housekeeping genes) to determine the fold change in gene expression between Wt and Abcd1 null mice.

Antibodies

The following antibodies were used for western blots: polyclonal phosphoserine 307 IRS1 antibody (07-247) and polyclonal IRS1 antibody (06-248) were obtained from Chemicon International (Temecula, CA, USA). Antibodies against SAPK/JNK (number 9252), Phospho-SAPK/JNK (Thr183-Tyr185) (9251), Akt (pan) (11E7) (4685), phospho-Akt (Ser473) (587F11) (4051), phospho-Akt (Thr308) (244F9) (4056), phospho p70S6K (Thr389) (9205), phospho-IKKα-Ser180/IKKβ-Ser181 (2681) were obtained from Cell Signaling (Beverly, MA, USA). Monoclonal phospho-Tyr (PY20) (sc-508), IκBα (sc-1643), IKKβ (sc-7330) and α-p52 (sc-7386) were purchased from Santa Cruz Biotechnology. IKKα (OP-133) was purchased from Oncogen and α-tubulin from Sigma. Goat anti-mouse-HRP secondary antibody was obtained from Invitrogen (Eugene, OR, USA).

Tissue extracts and western blot analysis

Spinal cord from control and X-ALD mice were collected, frozen in liquid nitrogen and stored at −70°C until further analysis. Fresh frozen spinal cords were homogenized in 5 vol of ice-cold lysis buffer (RIPA buffer: 25 mM Tris–HCl, pH 6, 150 mM NaCl, 1% NP-40, 1% sodium deoxycholate, 0.1% SDS with complete protease inhibitor cocktail (Roche) and phosphatase inhibitor cocktail (Roche) followed by sonication. Homogenates were centrifuged at 1000 rpm ×5′ at 4°C, and supernatants were collected. Protein concentration was assessed using bicinchoninic acid assay (Pierce, Rockford, IL, USA). Samples containing 50–75 μg of protein in reducing sample buffer were fractionated by sodium dodecyl sulfate–polyacrylamide gel electrophoresis. Proteins were transferred to Hybond-C nitrocellulose membranes and subjected to western blots with indicated antibodies followed by quantification by a scanning densitometer. Signals were normalized to loading controls.

Organotypic spinal cord slice culture

The spinal cords from 18-day-old mice were immediately removed and placed in ice-cold dissecting media (pH 7.15). Next, the spinal cord was cut into 350-mm thick slices using a McIlwain tissue chopper to generate the organotypic slice cultures and placed into a sterile Petri dish with Grey's balanced salt solution. Spinal slices were transferred onto Millicell-CM cultured plate inserts (Millipore, MA, USA). The inserts were placed into wells of a 6-well plate containing 1.0 ml of medium containing 50% MEM with Earl's salts and glutamine, 25% Hanks balanced salt solution and 25% horse serum supplemented with 20 mM of HEPES acid–salt and D-glucose (6 mg/ml) (Gibco-BRL). Slices were incubated at 37°C for different period of times and media were changed twice a week (56,57). After 2 weeks of culture, OSCSC have been treated with C26:0 fatty acid dissolved in ethanol (22).

SUPPLEMENTARY MATERIAL

Supplementary Material is available at *HMG* online.

FUNDING

REFERENCES

1. Ferrer, I., Aubourg, P. and Pujol, A. (2010) General aspects and neuropathology of X-linked adrenoleukodystrophy. *Brain Pathol.*, **20**, 817–830.
2. Mosser, J., Douar, A.M., Sarde, C.O., Kioschis, P., Feil, R., Moser, H., Poustka, A.M., Mandel, J.L. and Aubourg, P. (1993) Putative X-linked adrenoleukodystrophy gene shares unexpected homology with ABC transporters. *Nature*, **361**, 726–730.
3. van Roermund, C.W., Visser, W.F., Ijlst, L., van Cruchten, A., Boek, M., Kulik, W., Waterham, H.R. and Wanders, R.J. (2008) The human peroxisomal ABC half transporter ALDP functions as a homodimer and accepts acyl-CoA esters. *FASEB J.*, **22**, 4201–4208.
4. Kemp, S., Pujol, A., Waterham, H.R., van Geel, B.M., Boehm, C.D., Raymond, G.V., Cutting, G.R., Wanders, R.J. and Moser, H.W. (2001) ABCD1 mutations and the X-linked adrenoleukodystrophy mutation database: role in diagnosis and clinical correlations. *Hum. Mutat.*, **18**, 499–515.
5. Moser, H., Smith, K.D., Watkins, P.A., Powers, J. and Moser, A.B. (2001) In Scriver, C. (ed.), *The Metabolic and Molecular Bases of Inherited Disease*. McGraw-Hill, New York, pp. 3257–3301.
6. Asheuer, M., Bieche, I., Laurendeau, I., Moser, A., Hainque, B., Vidaud, M. and Aubourg, P. (2005) Decreased expression of ABCD4 and BG1 genes early in the pathogenesis of X-linked adrenoleukodystrophy. *Hum. Mol. Genet.*, **14**, 1293–1303.
7. Cartier, N., Hacein-Bey-Abina, S., Bartholomae, C.C., Veres, G., Schmidt, M., Kutschera, I., Vidaud, M., Abel, U., Dal-Cortivo, L., Caccavelli, L. et al. (2009) Hematopoietic stem cell gene therapy with a lentiviral vector in X-linked adrenoleukodystrophy. *Science*, **326**, 818–823.
8. Pujol, A., Ferrer, I., Camps, C., Metzger, E., Hindelang, C., Callizot, N., Ruiz, M., Pampols, T., Giros, M. and Mandel, J.L. (2004) Functional overlap between ABCD1 (ALD) and ABCD2 (ALDR) transporters: a therapeutic target for X-adrenoleukodystrophy. *Hum. Mol. Genet.*, **13**, 2997–3006.
9. Pujol, A., Hindelang, C., Callizot, N., Bartsch, U., Schachner, M. and Mandel, J.L. (2002) Late onset neurological phenotype of the X-ALD gene inactivation in mice: a mouse model for adrenomyeloneuropathy. *Hum. Mol. Genet.*, **11**, 499–505.
10. Forss-Petter, S., Werner, H., Berger, J., Lassmann, H., Molzer, B., Schwab, M.H., Bernheimer, H., Zimmermann, F. and Nave, K.A. (1997) Targeted inactivation of the X-linked adrenoleukodystrophy gene in mice. *J. Neurosci. Res.*, **50**, 829–843.
11. Lu, J.F., Lawler, A.M., Watkins, P.A., Powers, J.M., Moser, A.B., Moser, H.W. and Smith, K.D. (1997) A mouse model for X-linked adrenoleukodystrophy. *Proc. Natl Acad. Sci. USA*, **94**, 9366–9371.
12. Singh, I. and Pujol, A. (9999) Pathomechanisms underlying X-adrenoleukodystrophy: a three-hit hypothesis. *Brain Pathol.*, **20**, 838–844.
13. Ashburner, M., Ball, C.A., Blake, J.A., Botstein, D., Butler, H., Cherry, J.M., Davis, A.P., Dolinski, K., Dwight, S.S., Eppig, J.T. et al. (2000) Gene ontology: tool for the unification of biology. The Gene Ontology Consortium. *Nat. Genet.*, **25**, 25–29.
14. Kanehisa, M. and Goto, S. (2000) KEGG: Kyoto Encyclopedia of Genes and Genomes. *Nucleic Acids Res.*, **28**, 27–30.
15. Eichler, F.S., Ren, J.Q., Cossoy, M., Rietsch, A.M., Nagpal, S., Moser, A.B., Frosch, M.P. and Ransohoff, R.M. (2008) Is microglial apoptosis an early pathogenic change in cerebral X-linked adrenoleukodystrophy? *Ann. Neurol.*, **63**, 729–742.
16. Tilg, H. and Moschen, A.R. (2006) Adipocytokines: mediators linking adipose tissue, inflammation and immunity. *Nat. Rev. Immunol.*, **6**, 772–783.
17. Wymann, M.P. and Schneiter, R. (2008) Lipid signalling in disease. *Nat. Rev. Mol. Cell Biol.*, **9**, 162–176.
18. Aguirre, V., Werner, E.D., Giraud, J., Lee, Y.H., Shoelson, S.E. and White, M.F. (2002) Phosphorylation of Ser307 in insulin receptor substrate-1 blocks interactions with the insulin receptor and inhibits insulin action. *J. Biol. Chem.*, **277**, 1531–1537.
19. Gao, Z., Hwang, D., Bataille, F., Lefevre, M., York, D., Quon, M.J. and Ye, J. (2002) Serine phosphorylation of insulin receptor substrate 1 by inhibitor kappa B kinase complex. *J. Biol. Chem.*, **277**, 48115–48121.
20. Tsukumo, D.M., Carvalho-Filho, M.A., Carvalheira, J.B., Prada, P.O., Hirabara, S.M., Schenka, A.A., Araujo, E.P., Vassallo, J., Curi, R., Velloso, L.A. et al. (2007) Loss-of-function mutation in Toll-like receptor 4 prevents diet-induced obesity and insulin resistance. *Diabetes*, **56**, 1986–1998.
21. Um, S.H., Frigerio, F., Watanabe, M., Picard, F., Joaquin, M., Sticker, M., Fumagalli, S., Allegrini, P.R., Kozma, S.C., Auwerx, J. et al. (2004) Absence of S6K1 protects against age- and diet-induced obesity while enhancing insulin sensitivity. *Nature*, **431**, 200–205.
22. Fourcade, S., Lopez-Erauskin, J., Galino, J., Duval, C., Naudi, A., Jove, M., Kemp, S., Villarroya, F., Ferrer, I., Pamplona, R. et al. (2008) Early oxidative damage underlying neurodegeneration in X-adrenoleukodystrophy. *Hum. Mol. Genet.*, **17**, 1762–1773.
23. Hein, S., Schonfeld, P., Kahlert, S. and Reiser, G. (2008) Toxic effects of X-linked adrenoleukodystrophy-associated, very long chain fatty acids on glial cells and neurons from rat hippocampus in culture. *Hum. Mol. Genet.*, **17**, 1750–1761.
24. Galino, J., Ruiz, M., Fourcade, S., Schluter, A., Lopez-Erauskin, J., Guilera, C., Jove, M., Naudi, A., Garcia-Arumi, E., Andreu, A.L. et al. (2011) Oxidative damage compromises energy metabolism in the axonal degeneration mouse model of X-adrenoleukodystrophy. *Antioxid. Redox Signal*, **15**, 2095–2107.
25. Lopez-Erauskin, J., Fourcade, S., Galino, J., Ruiz, M., Schluter, A., Naudi, A., Jove, M., Portero-Otin, M., Pamplona, R., Ferrer, I. et al. (2011) Antioxidants halt axonal degeneration in a mouse model of X-adrenoleukodystrophy. *Ann. Neurol.*, **70**, 84–92.
26. Hooijmans, C.R. and Kiliaan, A.J. (2008) Fatty acids, lipid metabolism and Alzheimer pathology. *Eur. J. Pharmacol.*, **585**, 176–196.
27. Starkov, A.A., Fiskum, G., Chinopoulos, C., Lorenzo, B.J., Browne, S.E., Patel, M.S. and Beal, M.F. (2004) Mitochondrial alpha-ketoglutarate dehydrogenase complex generates reactive oxygen species. *J. Neurosci. Res.*, **24**, 7779–7788.
28. Gilg, A.G., Singh, A.K. and Singh, I. (2000) Inducible nitric oxide synthase in the central nervous system of patients with X-adrenoleukodystrophy. *J. Neuropathol. Exp. Neurol.*, **59**, 1063–1069.
29. Powers, J.M., Pei, Z., Heinzer, A.K., Deering, R., Moser, A.B., Moser, H.W., Watkins, P.A. and Smith, K.D. (2005) Adreno-leukodystrophy: oxidative stress of mice and men. *J. Neuropathol. Exp. Neurol.*, **64**, 1067–1079.
30. Bernheimer, H., Budka, H. and Muller, P. (1983) Brain tissue immunoglobulins in adrenoleukodystrophy: a comparison with multiple sclerosis and systemic lupus erythematosus. *Acta Neuropathol.*, **59**, 95–102.
31. Ho, J.K., Moser, H., Kishimoto, Y. and Hamilton, J.A. (1995) Interactions of a very long chain fatty acid with model membranes and serum albumin: implications for the pathogenesis of adrenoleukodystrophy. *J. Clin. Invest.*, **96**, 1455–1463.
32. Powers, J.M. and Moser, H.W. (1998) Peroxisomal disorders: genotype, phenotype, major neuropathologic lesions, and pathogenesis. *Brain Pathol.*, **8**, 101–120.
33. Boden, G., She, P., Mozzoli, M., Cheung, P., Gumireddy, K., Reddy, P., Xiang, X., Luo, Z. and Ruderman, N. (2005) Free fatty acids produce

insulin resistance and activate the proinflammatory nuclear factor-kappaB pathway in rat liver. *Diabetes*, **54**, 3458–3465.

34. Griffin, M.E., Marcucci, M.J., Cline, G.W., Bell, K., Barucci, N., Lee, D., Goodyear, L.J., Kraegen, E.W., White, M.F. and Shulman, G.I. (1999) Free fatty acid-induced insulin resistance is associated with activation of protein kinase C theta and alterations in the insulin signaling cascade. *Diabetes*, **48**, 1270–1274.

35. Evans, J.L., Maddux, B.A. and Goldfine, I.D. (2005) The molecular basis for oxidative stress-induced insulin resistance. *Antioxid. Redox Signal*, **7**, 1040–1052.

36. Singh, J., Khan, M. and Singh, I. (2009) Silencing of *Abcd1* and *Abcd2* genes sensitizes astrocytes for inflammation: implication for X-adrenoleukodystrophy. *J Lipid Res.*, **50**, 135–147.

37. Henkel, J.S., Beers, D.R., Siklos, L. and Appel, S.H. (2006) The chemokine MCP-1 and the dendritic and myeloid cells it attracts are increased in the mSOD1 mouse model of ALS. *Mol. Cell. Neurosci.*, **31**, 427–437.

38. Henkel, J.S., Engelhardt, J.I., Siklos, L., Simpson, E.P., Kim, S.H., Pan, T., Goodman, J.C., Siddique, T., Beers, D.R. and Appel, S.H. (2004) Presence of dendritic cells, MCP-1, and activated microglia/macrophages in amyotrophic lateral sclerosis spinal cord tissue. *Ann. Neurol.*, **55**, 221–235.

39. Hotamisligil, G.S. (2006) Inflammation and metabolic disorders. *Nature*, **444**, 860–867.

40. Shi, H., Kokoeva, M.V., Inouye, K., Tzameli, I., Yin, H. and Flier, J.S. (2006) TLR4 links innate immunity and fatty acid-induced insulin resistance. *J. Clin. Invest.*, **116**, 3015–3025.

41. Cartier, N. and Aubourg, P. (2010) Hematopoietic stem cell transplantation and hematopoietic stem cell gene therapy in X-linked adrenoleukodystrophy. *Brain Pathol.*, **20**, 857–862.

42. Paintlia, A.S., Gilg, A.G., Khan, M., Singh, A.K., Barbosa, E. and Singh, I. (2003) Correlation of very long chain fatty acid accumulation and inflammatory disease progression in childhood X-ALD: implications for potential therapies. *Neurobiol. Dis.*, **14**, 425–439.

43. Wolf, A.M., Wolf, D., Rumpold, H., Enrich, B. and Tilg, H. (2004) Adiponectin induces the anti-inflammatory cytokines IL-10 and IL-1RA in human leukocytes. *Biochem. Biophys. Res. Commun.*, **323**, 630–635.

44. Yamaguchi, N., Argueta, J.G., Masuhiro, Y., Kagishita, M., Nonaka, K., Saito, T., Hanazawa, S. and Yamashita, Y. (2005) Adiponectin inhibits Toll-like receptor family-induced signaling. *FEBS Lett.*, **579**, 6821–6826.

45. Spranger, J., Verma, S., Gohring, I., Bobbert, T., Seifert, J., Sindler, A.L., Pfeiffer, A., Hileman, S.M., Tschop, M. and Banks, W.A. (2006) Adiponectin does not cross the blood–brain barrier but modifies cytokine expression of brain endothelial cells. *Diabetes*, **55**, 141–147.

46. Glezer, I., Lapointe, A. and Rivest, S. (2006) Innate immunity triggers oligodendrocyte progenitor reactivity and confines damages to brain injuries. *FASEB J.*, **20**, 750–752.

47. Fassbender, K., Walter, S., Kuhl, S., Landmann, R., Ishii, K., Bertsch, T., Stalder, A.K., Muehlhauser, F., Liu, Y., Ulmer, A.J. *et al.* (2004) The LPS receptor (CD14) links innate immunity with Alzheimer's disease. *FASEB J.*, **18**, 203–205.

48. Bate, C., Veerhuis, R., Eikelenboom, P. and Williams, A. (2004) Microglia kill amyloid-beta1–42 damaged neurons by a CD14-dependent process. *Neuroreport*, **15**, 1427–1430.

49. Yuan, M., Konstantopoulos, N., Lee, J., Hansen, L., Li, Z.W., Karin, M. and Shoelson, S.E. (2001) Reversal of obesity- and diet-induced insulin resistance with salicylates or targeted disruption of Ikkbeta. *Science*, **293**, 1673–1677.

50. Lunnon, K., Teeling, J.L., Tutt, A.L., Cragg, M.S., Glennie, M.J. and Perry, V.H. (2011) Systemic inflammation modulates Fc receptor expression on microglia during chronic neurodegeneration. *J. Immunol.*, **186**, 7215–7224.

51. Ferrer, I., Kapfhammer, J.P., Hindelang, C., Kemp, S., Troffer-Charlier, N., Broccoli, V., Callyzot, N., Mooyer, P., Selhorst, J., Vreken, P. *et al.* (2005) Inactivation of the peroxisomal ABCD2 transporter in the mouse leads to late-onset ataxia involving mitochondria, Golgi and endoplasmic reticulum damage. *Hum. Mol. Genet.*, **14**, 3565–3577.

52. Ghate, A., Befort, K., Becker, J.A., Filliol, D., Bole-Feysot, C., Demebele, D., Jost, B., Koch, M. and Kieffer, B.L. (2007) Identification of novel striatal genes by expression profiling in adult mouse brain. *Neuroscience*, **146**, 1182–1192.

53. Gentleman, R.C., Carey, V.J., Bates, D.M., Bolstad, B., Dettling, M., Dudoit, S., Ellis, B., Gautier, L., Ge, Y., Gentry, J. *et al.* (2004) Bioconductor: open software development for computational biology and bioinformatics. *Genome Biol.*, **5**, R80.

54. Smyth, G.K. (2005) In Gentleman, R., Carey, V., Dudoit, S., Irizarry, R. and Huber, W. (eds), *Bioinformatics and Computational Biology Solutions using R and Bioconductor*. Springer, New York, pp. 397–420.

55. Mootha, V.K., Lindgren, C.M., Eriksson, K.F., Subramanian, A., Sihag, S., Lehar, J., Puigserver, P., Carlsson, E., Ridderstrale, M., Laurila, E. *et al.* (2003) PGC-1alpha-responsive genes involved in oxidative phosphorylation are coordinately downregulated in human diabetes. *Nat. Genet.*, **34**, 267–273.

56. Krassioukov, A.V., Ackery, A., Schwartz, G., Adamchik, Y., Liu, Y. and Fehlings, M.G. (2002) An *in vitro* model of neurotrauma in organotypic spinal cord cultures from adult mice. *Brain Res. Brain Res. Protoc.*, **10**, 60–68.

57. Rothstein, J.D., Jin, L., Dykes-Hoberg, M. and Kuncl, R.W. (1993) Chronic inhibition of glutamate uptake produces a model of slow neurotoxicity. *Proc. Natl Acad. Sci. USA*, **90**, 6591–6595.